Response to reviewers for the paper "Technical Note: Effect of varying the λ = 185 and 254 nm photon flux ratio on radical generation in oxidation flow reactors."

We thank the referees for their comments on our paper. To guide the review process, we have copied the referee's comments in black text. Our responses are in blue text. We respond to Referee #1 and #2 comments, with alterations to the paper indicated in **bold or ~~struck through~~ text** below and in annotations to the revised manuscript.

Anonymous Referee #1

1. Page 2, line 35. I find this sentence a bit confusing. Specifically the statement that compressed air or O2 is not required for external O3 generation making the lamps with 185 nm easier to use in field studies. How are normally lamps with 185 nm used in the field? Just with ambient air? How a stable water vapor concentration is achieved?

We modified the text as follows:

P2, L35: "Additionally, OFR185 is often more practical than OFR254 to apply in field studies because **O_2 and H_2O that are already present in ambient air are photolyzed to generate O_3, OH and HO_2, whereas OFR254 requires addition of** compressed air or O_2 ~~is not required~~ for external O_3 generation **and additional inlet plumbing to inject it at the OFR inlet**."

2. Page2, line 49. Please add the specification of the sensor used to measure the relative humidity.

We modified the text as follows:

P2, L49: "A photodetector (TOCON-C6, sglux Gmbh) and a relative humidity and temperature (RH/T) sensor **(SHT21, Sensiron)** were mounted in the exit flange of the OFR."

3. Page 3, section 2.1. Here it is not clear how the choice of these lamps was made. I assume it was done to cover the largest possible range of I185:I254 ratios? Or are these lamps the most commonly used? I would suggest to extend a little bit the section to more clearly explain these lamps were used.

We modified the text as follows:

P3, L59: "Figure 1 shows the Hg fluorescent lamp configurations that were used in this study. Lamp type A is **an** ozone producing low-pressure Hg germicidal fluorescent lamp (GPH436T5VH/4P, Light Sources Inc.) in which quartz that transmits λ = 185 and 254 nm radiation is present along the entire 356 mm arc length. **This lamp type is a standard component of the Aerodyne PAM OFR.** The relative transmissivity of λ = 185 nm radiation (T185) in lamp type A is thus equal to 1. […] A different type of quartz is available that blocks λ = 185 nm and transmits λ =254 nm radiation (T_{185}=0). **To cover the largest possible range of I_{185}:I_{254},** Lamp types C, D, E […] fused one segment each of quartz with T185 = 0 and T185 = 1 to provide reduced I_{185} relative to lamp type A while maintaining constant I_{254}."

4. Page 7, code and availability. There it is stated that the KinSim mechanism is available upon request. Though, in the supplement of the paper (page 4) a table is listed with caption indicating that it contains the KinSim mechanism. So, which one was used within this study? I would

recommend including the one developed within the study in the supplement so that anyone could make use of it.

We will upload the KinSim mechanism that was used in this study to the Supplement materials.

Anonymous Referee #2

My major concerns/points to be addressed are:

1. The motivation behind using the estimation equation where six parameters are fitted. I assume the physical meaning behind all these parameters (factors) are described in Li et al but one can expect a short introduction to the equation also in this technical note to understand what are instrumental specifics and what are related to a general parametrization of the chemistry or physics.

We modified the text as follows:

P5, L140: "Previous studies reported empirical OH exposure algebraic estimation equations for use with OFRs […]. We adapted the estimation equation format introduced by Li et al. (2015):

$$\log[OH_{exp}] = \left(a + (b + c \times OHR_{ext}^{d} + e \times \log[O_3 \times OHR_{ext}^{f}]) \times \log[O_3] + \log[H_2O]\right) + \log\left(\frac{\tau}{124}\right) \quad (1)$$

This equation incorporates the following relationships between OH_{exp} and O_3, H_2O, τ and OHR_{ext} identified by Li et al. (2015): (1) a power-law dependence of OH_{exp} on UV intensity, and, accordingly, $[O_3]$; (2) a linear dependence of OH_{exp} on $[H_2O]$ and τ; (3) OH suppression as a function of increasing OHR_{ext}. The fit coefficents *a-f* are lamp-specific."

2. Clarify to what extent the information provided are limited to the OFRs designed and commercialized by aerodyne. Note: If the extent is significant I would suggest a short statement under "competing interests" according to the ACP policy.

We modified the text as follows:

P7, L191: "To develop a general framework within which to evaluate and compare different OFR185 systems, we characterized OH_{exp} as a function of I_{185}, I_{254}, OHR_{ext}, and $[H_2O]$ values, in the process using several novel low-pressure Hg lamp configurations to extend the range of achievable I_{185}:I_{254}. OH_{exp} estimation equations were developed for the Hg lamp types that were used, and corresponding estimation equation fit coefficients were parameterized as a function of I_{185}:I_{254} to enable interpolation to other OFR185 systems ~~that were not studied here~~ **that can employ the same Hg lamp type(s) over the range of $[O_3]$, $[H_2O]$, OHR_{ext} and τ values parameterized here. Because low-pressure Hg germicidal fluorescent lamps are used in many industries (e.g. medical, HVAC, wastewater remediation), they are less expensive and more easily acquired than other Hg lamps."**

3. The discussion on plug-flow condition. I assume one can give a more accurate description on the residence time distribution with measured data obtained from a pulse of an inert tracer compound.

We agree with the reviewer that the residence time distribution can be measured to within better than ± 30% uncertainty at a specific OFR condition. However, in our opinion, it is unlikely that such a measurement could be then accurately applied across many OFR conditions where parameters such as temperature vary due to ambient conditions or waste heat dissipation from lamps. For example, in Lambe et al. (2019), mean residence times obtained from pulsed tracer measurements at OFR temperatures of 22°C and 39°C were 120 ± 34 s and 98 ± 63 s during periods when the lamps were turned off and on respectively. Rather than making explicit RTD measurements across many OFR conditions, simply accepting ± 30% uncertainty in the residence time may be an acceptable alternative for many users.

To clarify this point in the manuscript, we revised the text as follows:

P3, L80: "In most experiments, the **calculated** mean residence time was τ_{OFR} = 124 s, which was **obtained** from the ratio of the internal OFR volume (≈ 13 L) and the total sample and makeup flow rate through the OFR (6.4 L min^{-1}). This calculation implicitly assumes plug flow conditions, with associated uncertainty of approximately 10% compared to an explicit residence time distribution measurement **at a specific OFR condition** (Li et al., 2015). **Variability in OFR parameters (e.g. temperature, flow rate) may increase the uncertainty in this assumption across a continuum of conditions (Huang et al., 2017; Lambe et al., 2019).** To characterize the uncertainty in **our** plug flow approximation **across multiple sample flow conditions**, we measured integrated OH exposure (OH_{exp}) values of 3.3×10^{11}, 7.8×10^{11}, and 2.0×10^{12} molecule cm^{-3} s at **sample flow rates of 12.5, 6.4 and 3.1 L min^{-1}**, respectively, using the tracer decay method (Sec.2.2) with the OFR operated at the same humidity and lamp intensity. Thus, perturbing the "plug flow" τOFR = 124 s by a factor of 2 in either direction changed OH_{exp} by factors of 2.36 and 2.56. Based on these results, an upper-limit estimated uncertainty in τ_{OFR} and corresponding OH_{exp} is approximately 30%."

The following citations will be added to References:

Huang, Y., Coggon, M. M., Zhao, R., Lignell, H., Bauer, M. U., Flagan, R. C., and Seinfeld, J. H.: The Caltech Photooxidation Flow Tube reactor: design, fluid dynamics and characterization, Atmos. Meas. Tech., 10, 839–867, https://doi.org/10.5194/amt-10-839-2017, 2017.

Lambe, A. T., Krechmer, J. E., Peng, Z., Casar, J., Carrasquillo, A. J., Raff, J. D., Jimenez, J. L., and Worsnop, D. R.: HO_x and NO_x production in oxidation flow reactors via photolysis of isopropyl nitrite, isopropyl nitrite-d_7, and 1,3-propyl dinitrite at λ = 254, 350, and 369 nm, *Atmos. Meas. Tech.*, 12, 299-311, https://doi.org/10.5194/amt-12-299-2019, 2019.

Minor edits/points:

4. Row 3: Add NO3 -radicals

We modified the text as follows:

P1, L3: "Oxidation flow reactors (OFRs) complement environmental smog chambers as a portable, low-cost technique for exposing atmospheric compounds to oxidants such as ozone (O_3), **nitrate (NO_3) radicals,** and hydroxyl (OH) radicals. "

5. Row 57: I assume this dimming voltage is arbitrary? Can it be described in a better way?

We modified the text as follows:

P3, L57: "The dimming voltage applied to the ballast ranged from 0.8 to 10 VDC. **Below ~0.8 VDC, the lamp output was unstable due to flickering, and 10 VDC was the maximum control voltage permitted by the ballast."**

6. Row 64: Specify the type of quartz.

We modified the text as follows:

P3, L59: "Figure 1 shows the Hg fluorescent lamp configurations that were used in this study. Lamp type A is a standard ozone producing low-pressure Hg germicidal fluorescent lamp […] in which **type 214** quartz that transmits λ = 185 and 254 nm radiation is present along the entire 356 mm arc length. […] A different type of quartz is available (**type 219**) that blocks λ = 185 nm and transmits λ =254 nm radiation (T_{185} =0)."

7. Row 75/76: Strange wording. For me this would be a "reference OH reactivity" using reactivity of known tracers. Replace "external" with "reference" or "tracer".

We prefer the term "external OH reactivity" to distinguish from "internal OH reactivity" associated with intrinsic OFR photochemical reactions such as OH + HO_2 and OH + OH.

8. Row 81: See major comment.

For reference, here is text on lines 80-82 of the discussion paper: "In most experiments, the mean residence time was τ_{OFR} = 124 s, which was calculated from the ratio of the internal OFR volume (≈ 13 L) and the total sample and makeup flow rate through the OFR (6.4 L min^{-1}). This calculation implicitly assumes plug flow conditions, with associated uncertainty of approximately 10% compared to an explicit residence time distribution measurement (Li et al., 2015b)."

We assume the referee is referring to their Comment #3 above, where they stated: "I assume one can give a more accurate description on the residence time distribution with measured data obtained from a pulse of an inert tracer compound." If that is the case, we refer the referee to our response to comment #3 by referee #2. If that is not the case, we invite the referee to clarify and/or submit a follow up comment that we can reply to.

9. Row 96: Strange wording. If I understand right the model was tuned or adjusted?

We modified the text as follows:

P4, L95: "For cases where [H_2O] ≤ 0.1% and the RH **sensor accuracy became a limiting factor, we systematically adjusted the [H_2O] value that was** input to the model **to a value between 0.01 and 0.1%** to ~~generate~~ **achieve** better ~~model:measurement~~ ~~OHexp~~ agreement **between measured and modeled OH_{exp}"**.

Row 139: How much of the findings is Hg-lamp specific? Is this deviation to be expected when changing lamps in an OFR?

On P5, L139, we hypothesized that the different apparent lamp power dependence on I_{185}:I_{254} between this study and Li et al. (2015) was "presumably due to differences in the specific Hg lamps and/or method of dimming used in the two studies." Thus, we agree with the referee's suggestion that the findings might be specific to the Hg lamp type, and we think the manuscript as written already acknowledges that possibility. Thus, we assume that the referee is hypothesizing that lamp-to-lamp variability within the

same lamp type could also contribute additional uncertainty. While that has not been systematically evaluated here, we modified the text as follows to account for that as a possible additional explanation:

P5, L137: "I_{185}: I_{254} = 0.00561 for lamp types C and F (blue symbols) fell within the envelope of I_{185}: I_{254} = 0.004 to 0.012 characterized by Li et al. (2015), with a lower apparent sensitivity of I_{185}:I_{254} to lamp power. This is presumably due to differences in the specific Hg lamp **type**s, **potential variability in lamp output within the same lamp type,** and/or method of dimming used in the two studies**.**

10. Row 165: Rephrase so it's clearer that HO2 and NOx in addition to OH increases.

We modified the text as follows:

P6, L165: "~~In addition to [OH],~~ [HO_2] and [NO_x] (with N_2O present) increase **along with [OH] as a function of** I_{185} (Fig. S4)."

11. Row 183: Provide the values of used cross-sections.

We modified the text as follows:

P7, L184: " Assuming upper limit ϕ_{185} = 1 and ϕ_{254} =1 values **(Atkinson, 1986), σ_{185} = 2.8*10^{-17} cm^2, and σ_{254} = 8.9*10^{-19} cm^2 (Dawes et al., 2017)**, $F_{photolysis,benzene}$ ≤ 0.26 and 0.07 at low and high I185:I254".

12. Row 202: the used KinSin mechanism is also available in the supplemental?

Please see our response to Comment #4 raised by Referee #1.

Technical Note: Effect of varying the λ = 185 and 254 nm photon flux ratio on radical generation in oxidation flow reactors

Jake P. Rowe[1,+,*], Andrew T. Lambe[2,*], and William H. Brune[1]

[1]Department of Meteorology and Atmospheric Science, Pennsylvania State University, University Park, PA, USA
[2]Center for Aerosol and Cloud Chemistry, Aerodyne Research Inc., Billerica, MA, USA
[+]Now at: Department of Chemistry, University of Colorado, Boulder, CO, USA
[*]These authors contributed equally to this work.

Correspondence: Andrew T. Lambe (lambe@aerodyne.com)

Abstract.

Oxidation flow reactors (OFRs) complement environmental smog chambers as a portable, low-cost technique for exposing atmospheric compounds to oxidants such as ozone (O_3), nitrate (NO_3) radicals, and hydroxyl (OH) radicals. OH is most commonly generated in OFRs via photolysis of externally added O_3 at λ=254 nm (OFR254), or combined photolysis of O_2 and H_2O at λ = 185 nm plus photolysis of O_3 at λ=254 nm (OFR185) using low-pressure mercury (Hg) lamps. Whereas OFR254 radical generation is influenced by [O_3], [H_2O], and photon flux at λ = 254 nm (I_{254}), OFR185 radical generation is influenced by [O_2], [H_2O], I_{185}, and I_{254}. Because the ratio of photon fluxes, I_{185}:I_{254}, is OFR-specific, OFR185 performance varies between different systems even when constant H_2O and I_{254} are maintained. Thus, calibrations and models developed for one OFR185 system may not be applicable to another. To investigate these issues, we conducted a series of experiments in which I_{185}:I_{254} emitted by Hg lamps installed in an OFR was systematically varied by fusing multiple segments of lamp quartz together that either transmitted or blocked λ = 185 nm radiation. Integrated OH exposure (OH_{exp}) values achieved for each lamp type were obtained using the tracer decay method as a function of UV intensity, humidity, residence time, and external OH reactivity (OHR_{ext}). Following previous related studies, a photochemical box model was used to develop a generalized OH_{exp} estimation equation as a function of [H_2O], [O_3] and OHR_{ext} that is applicable for I_{185}:I_{254} $\approx$ 0.001 to 0.1.

1 Introduction

Hydroxyl (OH) radicals govern the concentrations of most atmospheric organic compounds, including those that lead to secondary organic aerosol (SOA) formation. For decades, environmental chambers and oxidation flow reactors (OFRs) have been used to simulate atmospheric aging processes through the controlled exposure of trace gases and aerosols to OH radicals. Environmental chamber studies are typically conducted over experimental timescales and equivalent atmospheric exposure times of hours up to 1 or 2 days. OFRs with residence times on the order of minutes achieve multiple days of equivalent atmospheric OH exposure (OH_{exp}), typically through the reactions

$$O_3 + h\nu_{254} \rightarrow O_2 + O(^1D) \quad \text{(R1)}$$

$$O(^1D) + H_2O \rightarrow 2OH \quad \text{(R2)}$$

$$O(^1D) + N_2O \rightarrow 2NO \quad \text{(R3)}$$

This method is referred to as OFR254, and relies on addition of externally generated O_3 at the OFR inlet. In some cases, OFRs have additionally employed the secondary λ = 185 nm emission line present in low-pressure mercury (Hg) lamps to generate radicals from the following reactions in addition to those listed above that are employed in OFR254:

$$H_2O + h\nu_{185} \rightarrow H + OH \quad \text{(R4)}$$

$$H + O_2 \rightarrow HO_2 \quad \text{(R5)}$$

$$O_2 + h\nu_{185} \rightarrow 2O(^3P) \quad \text{(R6)}$$

$$O(^3P) + O_2 \rightarrow O_3 \quad \text{(R7)}$$

$$N_2O + h\nu_{185} \rightarrow N_2 + O(^1D) \quad \text{(R8)}$$

This method is referred to as OFR185. Recent modeling studies suggest that OFR185 is less affected by experimental artifacts than OFR254 such as SOA photolysis and unwanted reactions with non-OH oxidants (Peng et al., 2016, 2018, 2019). Additionally, OFR185 is often more practical than OFR254 to apply in field studies because O_2 and H_2O that are already present in ambient air are photolyzed to generate O_3, OH and HO_2, whereas OFR254 requires addition of compressed air or O_2 ~~is not required~~ for external O_3 generation and additional inlet plumbing to inject it at the OFR inlet. However, because the λ = 185 nm photon flux (I_{185}) is influenced by OFR-specific design considerations that are mainly related to the Hg lamps being used, concentrations of O_3, HO_x = OH + HO_2 and NO_x = NO + NO_2 generated using OFR185 are potentially variable between different systems even when constant H_2O, N_2O and I_{254} are established. Thus, calibrations and models developed for one OFR185 system may not be applicable to another, making it more difficult to evaluate results or plan experiments. To investigate these issues, we designed a series of experiments in which I_{185}:I_{254} was systematically varied over a wide range using multiple novel Hg lamp configurations. Integrated OH_{exp} values were obtained as a function of OFR185 conditions, and a photochemical box model was used to develop a system of OH_{exp} estimation equations that are applicable to OFR185 systems with I_{185}:$I_{254} \approx 0.001$ to 0.1.

2 Experimental

Experiments were conducted using an Aerodyne Potential Aerosol Mass (PAM) OFR, which is a horizontal aluminum cylindrical chamber (46 cm long $\times$ 22 cm ID) operated in continuous flow mode (Lambe et al., 2011). A simplified schematic is shown in Figure S1. The H_2O mixing ratio in the OFR was controlled by passing the carrier gas through a Nafion humidifier (Perma Pure LLC) or heated recirculating water bath (Neslab Instruments, Inc.) and then diluting with different levels of dry

carrier gas at the OFR inlet. A photodetector (TOCON-C6, sglux Gmbh) and a relative humidity and temperature (RH/T) sensor (SHT21, Sensiron) were mounted in the exit flange of the OFR. Across all experiments, [H_2O] ranged from 0.03% (1% RH at 25.3 °C) to 3.9% (88% RH at 30.9 °C). The O_3 mixing ratio at the exit of the OFR was measured with a UV ozone analyzer (106-M, 2B Technologies).

2.1 HO_x generation

HO_x was produced via reactions R1-R2 and R4-R7. Photolysis of H_2O, O_2 and O_3 in the OFR was achieved using two low-pressure Hg fluorescent lamps (Light Sources, Inc.) that were isolated from the sample flow using type 214 quartz sleeves. Nitrogen purge gas was flowed over the lamps to prevent O_3 buildup between the lamps and sleeves. A fluorescent dimming ballast was used to regulate current applied to the lamps. The dimming voltage applied to the ballast ranged from 0.8 to 10 VDC. Below ~0.8 VDC, the lamp output was unstable due to flickering, and 10 VDC was the maximum control voltage permitted by the ballast.

Figure 1 shows the Hg fluorescent lamp configurations that were used in this study. Lamp type A is ~~a standard~~ an ozone-producing low-pressure Hg germicidal fluorescent lamp (GPH436T5VH/4P, Light Sources Inc.) in which type 214 quartz that transmits λ = 185 and 254 nm radiation is present along the entire 356 mm arc length. This lamp type is a standard component of the Aerodyne PAM OFR. The relative transmissivity of λ = 185 nm radiation (T_{185}) in lamp type A is thus equal to 1. Lamp type B is equivalent to lamp type A with added segments of opaque heat shrink tubing applied to approximately 86% of the arc length ($T_{185} \approx 0.14$; see also Fig. S2) to reduce I_{185} and I_{254} to levels below what is achievable using the ballast dimming voltage. A different type of quartz is available (type 219) that blocks λ = 185 nm and transmits λ = 254 nm radiation ($T_{185} = 0$). ~~Lamp~~ To cover the largest possible range of I_{185}:I_{254}, lamp types C, D, E (GPH436T5L/VH/4P 90/10, GPH436T5L/VH/4P 96/4, GPH436T5L/VH/4P 98.5/1.5; Light Sources, Inc.) fused one segment each of quartz with $T_{185} = 0$ and $T_{185} = 1$ to provide reduced I_{185} relative to lamp type A while maintaining constant I_{254}. Finally, to evaluate the effect of lamp design at fixed T_{185} and I_{254}, lamp types F and G contain the same ratios of $T_{185} = 0$ and $T_{185} = 1$ quartz as Types C and D, but with 5 and 13 total segments instead of 2 segments. These different designs isolate the effect of discretized λ = 185 nm irradiation across the entire arc length of the lamp versus having all λ = 185 nm radiation near the entrance of the OFR.

2.2 OH_{exp} characterization studies

OH_{exp}, defined here as the product of the average OH concentration and the mean OFR residence time (τ_{OFR}), was characterized by measuring the decay of carbon monoxide (CO) and/or sulfur dioxide (SO_2) tracers using Thermo 48i and 43i CO and SO_2 analyzers (e.g. Lambe et al. (2011)). Tracer mixing ratios entering the reactor were 6-9 ppmv for CO and 288-629 ppbv for SO_2, each diluted from separate gas mixtures of 0.5% CO or SO_2 in N_2 (Praxair). The corresponding total external OH reactivity (OHR_{ext}), which is the summed product of each tracer mixing ratio and its bimolecular OH rate coefficient, ranged from approximately 9 to 64 s^{-1}. Tracer concentrations were allowed to stabilize before initiating OH_{exp} measurements, during which steady-state levels of CO and/or SO_2 were obtained with the lamps turned off. Then, the lamps were turned on, and tracer concentrations were allowed to equilibrate before being measured at illuminated steady-state conditions.

In most experiments, the calculated mean residence time was τ_{OFR} = 124 s, which was ~~calculated~~ obtained from the ratio of the internal OFR volume (≈ 13 L) and the total sample and makeup flow rate through the OFR (6.4 L min $^{-1}$). This calculation implicitly assumes plug flow conditions, with associated uncertainty of approximately 10% compared to an explicit residence time distribution measurement ~~(Li et al., 2015b).~~ at a specific OFR condition (Li et al., 2015a). Variability in OFR parameters (e.g. temperature, flow rate) may increase the uncertainty in this assumption across a continuum of conditions (Huang et al., 2017; Lambe et al., 2019). To characterize the uncertainty in ~~the~~ our plug flow approximation ~~in our work, in a subset of experiments, τ_{OFR} ≈ 63 and 251 s were achieved by systematically changing the sample flow rate to 12.5 and 3.1 L min $^{-1}$. At τ_{OFR} = 63, 124, and 251 s,~~ across multiple sample flow conditions, we measured integrated OH exposure (OH_{exp}) values of 3.3×10^{11}, 7.8×10^{11}, and 2.0×10^{12} molecule cm^{-3} s at sample flow rates of 12.5, 6.4, and 3.1 L min^{-1}, respectively, using the tracer decay method (Sec. 2.2) with the OFR operated at the same humidity and lamp intensity. Thus, perturbing the "plug flow" τ_{OFR} = 124 s by a factor of 2 in either direction changed OH_{exp} by factors of 2.36 and 2.56. Based on these results, an upper-limit estimated uncertainty in τ_{OFR} and corresponding OH_{exp} is approximately 30%.

2.3 Photochemical model

We used a photochemical model implemented in MATLAB and Igor Pro to calculate concentrations of radical/oxidant species produced in the reactor ~~(Li et al., 2015b)~~(Li et al., 2015a). The KinSim chemical kinetic solver was used to compile the version of the model that was implemented in Igor Pro (Peng and Jimenez, 2019). Model input parameters are shown in Table 1, and reactions and associated kinetic rate coefficients that were included in the model are summarized in Table S1 (Peng and Jimenez, 2020). For cases where $[H_2O] \leq 0.1\%$ and the RH ~~was comparable to the accuracy of the measurement (± 2% RH), sensor accuracy became a limiting factor, we systematically adjusted the~~ $[H_2O]$ value that was input to the model ~~was varied~~ to a value between 0.01% and 0.1% to ~~generate better model:measurement~~ achieve better agreement between measured and modeled OH_{exp} ~~agreement~~. I_{254} and I_{185} values input to the model were adjusted to match the measured OH_{exp} values as best as possible within the following constraints:

1. $I_{254,max}$ = (3.5 ± 0.7)×10^{15} photons cm^{-2} s^{-1} for two lamps operated at maximum output (Lambe et al., 2019).
2. At reduced lamp output, I_{254} was calculated by multiplying $I_{254,max}$ by the ratio of photodetector-measured irradiance values measured at maximum and reduced lamp output at λ = 254 nm.
3. $I_{185,max}$:$I_{254,max}$ $\lessapprox$ 0.10 for lamp types A and B only ~~(Spicer, 2013).~~ (Spicer, 2013).
4. $I_{185,max}$:$I_{254,max}$ $\lessapprox$ 0.01, 0.004, and 0.0015 for lamp types C and F, D and G, and E, respectively.
5. At reduced lamp output, I_{185} was calculated by multiplying $I_{185,max}$ by the ratio of O_3 mixing ratios measured at maximum and reduced lamp output.

Within these constraints, the mean (± 1σ) ratios of modeled:measured CO and SO_2 concentrations remaining at the exit of the OFR were 1.02±0.06 and 0.97±0.17, respectively.

3 Results and Discussion

3.1 Influence of I_{185} on $[O_3]$ and OH_{exp}

Figure 2 shows $[O_3]$ measured at the exit of the OFR as a function of T_{185} with each lamp type operated at maximum UV output. Binned data are shown for conditions where $[H_2O]$ = 0.15±0.11%, 0.98±0.08%, 1.74±0.23%, and 3.42±0.30%. At fixed $[H_2O]$, $[O_3]$ increased as a function of T_{185}. For example, $[O_3]$ increased from 17.8 to 155 ppmv at $[H_2O]$ = 0.15% and from 4.5 to 56 ppmv at $[H_2O]$ = 1.74% as T_{185} increased from 0.1 to 1. At fixed T_{185} and I_{254}, $[O_3]$ decreased with increasing $[H_2O]$ due to faster $O(^1D)$ + H_2O reaction rate following O_3 photolysis at λ = 254 nm. Consequently, as $[H_2O]$ increased from 0.15 to 3.42%, $[O_3]$ decreased by a factor of 4-5 for lamp types A and C-G, whereas $[O_3]$ decreased by a factor of 2 for lamp type B because of its reduced I_{254} (Fig. 1). At $[H_2O]$ = 1.74% and T_{185} = 0.04 and 0.1, Figure 2, shows that $[O_3]$ generated using lamp types D and G was approximately 1.7 and 1.8 ppmv; here, lamp type D had one 15 mm quartz segments with T_{185} = 1, whereas lamp type G had three 5 mm quartz segments with T_{185} = 1. At the same OFR conditions, $[O_3]$ generated using lamp types C and F was 4.5 and 2.7 ppmv; these lamps had one 35 mm and seven 5 mm quartz segments with T_{185} = 1. Despite the discrepancy in measured $[O_3]$, corresponding OH_{exp} obtained with lamp types C and F were 2.5×10^{12} and 2.8×10^{12} molecules cm^{-3} s respectively. Thus, the worse agreement in $[O_3]$ measured between lamp types C and F may be associated specifically with O_3 measurements from these experiments. We hypothesize that the OFR-volume-averaged I_{185} is sufficient to describe associated HO_x production for these cases.

Figure 3 plots OH_{exp} as a function of T_{185} at $[H_2O]$= 1.90±0.26%. The corresponding equivalent photochemical age shown on the right y-axis assumes a 24-hour average OH concentration of 1.5×10^6 molec cm^{-3} (Mao et al., 2009). Results obtained with lamp types D & G and C & F were averaged together at T_{185} = 0.04 and 0.1 respectively due to their similar OH_{exp} values. Over the range of T_{185} shown in Fig. 3, excluding lamp type B, OH_{exp} increased by approximately a factor of 5 at I_{254} = $(3.7\pm0.6)\times10^{15}$ photons cm^{-2} s^{-1}) and a factor of 17 at I_{254} = $(2.1\pm0.3)\times10^{14}$ photons cm^{-2} s^{-1}. Maximum OH_{exp} also decreased by about a factor of 5 between lamp types A and B due to reduction in both I_{254} and I_{185} (not shown in Fig. 3). Similar trends were observed for OH_{exp} measurements at $[H_2O]$ = 0.93±0.06% and 3.42±0.30%, but at $[H_2O]$ = 0.09±0.07%, the sensitivity of OH_{exp} to T_{185} was weaker due to suppressed OH production at lower humidity.

3.2 I_{185}:I_{254} determination and derivation of OH_{exp} estimation equations

Figure 4 plots I_{185} as a function of I_{254} for the Hg lamps used in this study and a different model of Hg lamps used in an earlier-generation PAM OFR (Li et al., 2015a). As with OH_{exp} values shown in Fig. 3, I_{185} and I_{254} values obtained with lamp types D & G and C & F were combined together into T_{185} = 0.04 and 0.1 symbols following our hypothesis that the OFR-volume-averaged I_{185} was sufficient to describe HO_x production. Linear fits applied to the data shown in Fig. 4 were used to calculate average I_{185}: I_{254} values for lamp types A & B, C & F, D & G, and E. Lamp types A and B (red symbols) had the highest I_{185}: I_{254} = 0.0664, whereas lamp type E had the lowest I_{185}: I_{254} = 0.00167. I_{185}: I_{254} = 0.00561 for lamp types C and F (blue symbols) fell within the envelope of I_{185}: I_{254} = 0.004 to 0.012 characterized by Li et al. (2015a), with

a lower apparent sensitivity of I_{185}: I_{254} to lamp power. This is presumably due to differences in the specific Hg ~~lamps~~ lamp types,potential variability in lamp output within the same lamp type, and/or method of dimming used in the two studies.

Previous studies reported empirical OH exposure algebraic estimation equations for use with OFRs (Li et al., 2015a; Peng et al., 2015, 2018; Lambe et al., 2019). These equations parameterize OH_{exp} as a function of readily-measured experimental parameters, therefore providing a simpler alternative than detailed photohemical models for experimental planning and analysis. Here, we expand on those studies by deriving OH_{exp} estimation equations for the lamp types that were used in this study. We adapted the estimation equation format introduced by Li et al. (2015a):

$$\log[OH_{exp}] = \left(a + (b + c \times OHR_{ext}^{d} + e \times \log[O_3 \times OHR_{ext}^{f}]) \times \log[O_3] + \log[H_2O]\right) + \log\left(\frac{\tau}{124}\right) \quad (1)$$

This equation incorporates the following relationships between OH_{exp} and O_3, H_2O, τ and OHR_{ext} identified by (Li et al., 2015a) : (1) a power-law dependence of OH_{exp} on UV intensity, and, accordingly, $[O_3]$; (2) a linear dependence of OH_{exp} on $[H_2O]$ and τ; (3) OH suppression as a function of increasing OHR_{ext}. The fit coefficents *a-f* are lamp-specific.

Equation 1 was fit to data obtained from the base case of the model, with CO reacting with OH as a surrogate of OHR_{ext}, over the following OFR185 phase space: T = 25°C, τ = 124 s, OHR_{ext} = 0.77 to 232 s^{-1}, $[H_2O]$ = 0.1 to 3%, I_{254} = 10^{13} to 10^{16} photons cm^{-2} s^{-1}, and I_{185}:I_{254} = 0.00167, 0.00242, 0.00595, and 0.0664. For each I_{185}:I_{254} value, we explored 10, 15, and 20 logarithmically evenly distributed values in the ranges of OHR_{ext}, $[H_2O]$, and I_{254}, respectively. Figure 5 compares OH_{exp} estimated from Eq. 1 and calculated from the model for the I_{185}:I_{254} = 0.0664 case. Almost all of the equation-estimated and model OH_{exp} values agreed within a factor or 2 or better. The absolute value of the relative deviations increased above $[H_2O] \approx 0.5\%$ and was largest at $[H_2O]$ =3%; the mean absolute value of the relative devations was 28%. Analogous plots for I_{185}:I_{254} = 0.00167, 0.00242, and 0.00595 cases are shown in Fig. S3. For these other cases, the mean absolute values of the relative deviations were 20%, 17% and 16%, respectively. Eq. 1 coefficients for lamps with the I_{185}: I_{254} values reported here are presented in Table 2.

To generalize the results shown in Figs. 5 and S3 to OFR185 systems with other I_{185}: I_{254} values, Figure 6 plots fit coefficients *a* - *f* as a function of I_{185}: I_{254}. Each of these coefficients changes monotonically as a function of I_{185}: I_{254}, enabling the usage of simple exponential regression functions to parameterize the *a* - *f* values as a continuous function of I_{185}: I_{254}. Exponential function coefficients for the regression curves shown in Fig. 6 are presented in Table 3. Figure 7 compares the equation-estimated OH_{exp} (obtained using Eq. 1 with Table 3 fit coefficients) and the measured OH_{exp} obtained using the tracer decay method. The mean ($\pm 1\sigma$) ratios of equation-estimated and measured OH_{exp} values were 0.94±0.55, 1.13±0.48, 1.03±0.37, and 1.32±0.71 for I_{185}:I_{254} = 0.00167, 0.00242, 0.00595, and 0.0664.

3.3 Influence of I_{185} on HO_2, NO_x, and UV photolysis of aromatic volatile organic compounds

~~In addition to~~ [~~OH,~~ HO_2] and [NO_x] (with N_2O present) ~~also increase with increasing~~ increase along with [OH] as a function of I_{185} (Fig. S4). To isolate the effect of I_{185} on related OFR photochemistry at fixed OH_{exp}, we investigated two OFR185 cases using (I_{185},I_{254}) = (3.33×10^{12}, 1.96×10^{15}) and (6.65×10^{12}, 1.01×10^{14}) photons cm^{-2} s^{-1} that each generate a model-calculated OH_{exp} = 5.0×10^{11} molecules cm^{-3} s at base case conditions of $[H_2O]$ = 2%, τ = 124 s, and OHR_{ext} = 30 s^{-1}.

These cases were designated as "low" and "high" I_{185}:I_{254} cases. Thus, increasing I_{185} by a factor of 2 enabled lowering I_{254} by a factor of 20 to achieve equivalent OH_{exp}.

First, we investigated the resilience of each OFR185 case to OH suppression via OHR_{ext}. As OHR_{ext} was increased from 30 to 300 s^{-1}, OH_{exp} decreased from 5.0×10^{11} to 7.9×10^{10} (low I_{185}:I_{254}) and 9.0×10^{10} (high I_{185}:I_{254}) molecules cm^{-3} s^{1}. Thus, increasing I_{185} decreased OH suppression by 15%, primarily due to 30% higher [HO_2] in the high I_{185}:I_{254} case that increased the OH + HO_2 reaction rate and partially buffered the system against increasing OHR_{ext}. Second, we compared the ability of each OFR185 case to generate high-NO conditions in the presence of added [N_2O]. For example, at [N_2O] = 2.7%, NO:HO_2 = 1 and 0.4 at low and high I_{185}:I_{254}. While increasing [N_2O] from 2.7% to 4.0% achieved NO:HO_2 = 1 at high I_{185}:I_{254}, [NO_2] also increased from 50 to 100 ppbv. At higher UV intensity, a similar increase in [N_2O] could generate [NO_2] $>$ 1 ppm and promote artificially fast RO_2 + NO_2 reactions compared to atmospheric conditions (Peng and Jimenez, 2017). Third, we compared relative timescales for OH oxidation and photolysis of representative aromatic volatile organic compounds (VOCs) that absorb λ = 185 and 254 nm radiation. The fractional VOC loss due to photolysis, $F_{photolysis}$, was calculated using Equation 2:

$$F_{photolysis} = \frac{\sigma_{185}I_{185}\phi_{185} + \sigma_{254}I_{254}\phi_{254}}{\sigma_{185}I_{185} \times \phi_{185} + \sigma_{254}I_{254}\phi_{254} + k_{OH}[OH]} \quad (2)$$

Where σ_{185} and σ_{254} are the VOC absorption cross sections at λ = 185 and 254 nm, ϕ_{185} and ϕ_{254} are the VOC photolysis quantum yields, and k_{OH} is the bimolecular reaction rate coefficient with OH. Assuming upper limit ϕ_{185} = 1 and ϕ_{254} =1 values, σ_{185} = 2.8×10^{-17} cm^2 and σ_{254} = 8.9×10^{-19} cm^2 (Dawes et al., 2017), and k_{OH} = 1.28×10^{-12} cm^3 $molec^{-1}$ s^{-1} (Atkinson, 1986), $F_{photolysis,benzene} \leq$ 0.26 and 0.07 at low and high I_{185}:I_{254}~~(Atkinson, 1986; Dawes et al., 2017).~~. Similarly, $F_{photolysis,toluene} \leq$ 0.07 and 0.04 at low and high I_{185}:I_{254} (Atkinson, 1986; Serralheiro et al., 2015).

4 Conclusions

OFR185 is emerging as one of the most commonly used OFR methods by enabling efficient HO_x and NO_x generation over a range of oxidative aging timescales that are relevant to atmospheric processes.. Important OFR185 parameters are I_{185}, I_{254}, [H_2O], [N_2O] (if NO_x generation is required), OHR_{ext}, and τ_{OFR}. However, I_{185}:I_{254} is specific to the Hg lamp and/or OFR, as are associated calibration and estimation equations. To develop a general framework within which to evaluate and compare different OFR185 systems, we characterized OH_{exp} as a function of I_{185}, I_{254}, OHR_{ext}, and [H_2O] values, in the process using several novel low-pressure Hg lamp configurations to extend the range of achievable I_{185}:I_{254}. OH_{exp} estimation equations were developed for the Hg lamp types that were used, and corresponding estimation equation fit coefficients were parameterized as a function of I_{185}:I_{254} to enable interpolation to other OFR185 systems that ~~were not studied here.~~ can employ the same Hg lamp type(s) over the range of [O_3], [H_2O], OHR_{ext} and τ values parameterized here. Because low-pressure Hg germicidal fluorescent lamps are used in many industries (e.g. medical, HVAC, wastewater remediation), they are less expensive and more easily acquired than other Hg lamps.. OHR_{int}, HO_2:OH, and $F_{photolysis}$ were improved at higher I_{185}:I_{254}, whereas NO:HO_2 and NO:NO_2 were improved at lower I_{185}:I_{254}. Overall, our results suggest that optimal OFR185 performance is achieved by

(1) maximizing I_{185}:I_{254} (2) reducing OH_{exp} (if needed) through simultaneous reduction in I_{185} and I_{254} via electronically or mechanically dimming the lamp output (Fig. S2) (3) increasing $[N_2O]$ to offset higher $[HO_2]$ if high-NO conditions are required, provided that $[NO_2]$ does not exceed $\approx$ 1 ppm, in which case lower I_{185}:I_{254} should be used. Future work will investigate the sensitivitiy of NO_x-dependent, OH-initiated OVOC and SOA formation processes to I_{185}:I_{254}.

Code and data availability. Data presented in this paper are available upon request. The KinSim mechanism can be downloaded from the Supplement. kinetic solver is freely available at : https://tinyurl.com/kinsim-cases#bookmark=kix.6zu8zdwq2lce.

Author contributions. AL conceived and planned the experiments. JR performed the experiments. JR and AL performed the data analysis. JR, AL, and WB conceived and planned the model simulations, and JR and AL carried out the model simulations. JR, AL and WB contributed to the interpretation of the results. AL took the lead in writing the paper. All authors provided feedback on the paper.

Competing interests. The authors declare no competing interests.

Acknowledgements. We thank Chris Rockett (Light Sources Inc.), Dan Spicer (Light Sources Inc.), Leah Williams (Aerodyne), and John Jayne (Aerodyne) for helpful discussions.

References

Atkinson, R.: Kinetics and mechanisms of the gas-phase reactions of the hydroxyl radical with organic compounds under atmospheric conditions, Chemical Reviews, 86, 69–201, 1986.

Dawes, A., Pascual, N., Hoffmann, S. V., Jones, N. C., and Mason, N. J.: Vacuum ultraviolet photoabsorption spectroscopy of crystalline and amorphous benzene, Phys. Chem. Chem. Phys., 19, 27 544–27 555, http://dx.doi.org/10.1039/C7CP05319C, 2017.

Huang, Y., Coggon, M. M., Zhao, R., Lignell, H., Bauer, M. U., Flagan, R. C., and Seinfeld, J. H.: The Caltech Photooxidation Flow Tube reactor: design, fluid dynamics and characterization, Atmospheric Measurement Techniques, 10, 839–867, https://doi.org/10.5194/amt-10-839-2017, https://www.atmos-meas-tech.net/10/839/2017/, 2017.

Lambe, A. T., Ahern, A. T., Williams, L. R., Slowik, J. G., Wong, J. P. S., Abbatt, J. P. D., Brune, W. H., Ng, N. L., Wright, J. P., Croasdale, D. R., Worsnop, D. R., Davidovits, P., and Onasch, T. B.: Characterization of aerosol photooxidation flow reactors: heterogeneous oxidation, secondary organic aerosol formation and cloud condensation nuclei activity measurements, Atmospheric Measurement Techniques, 4, 445–461, 2011.

Lambe, A. T., Krechmer, J. E., Peng, Z., Casar, J. R., Carrasquillo, A. J., Raff, J. D., Jimenez, J. L., and Worsnop, D. R.: HO_x and NO_x production in oxidation flow reactors via photolysis of isopropyl nitrite, isopropyl nitrite-d_7, and 1,3-propyl dinitrite at $\lambda = 254$, 350, and 369 nm, Atmospheric Measurement Techniques, 12, 299–311, https://doi.org/10.5194/amt-12-299-2019, 2019.

Li, R., Palm, B. B., Ortega, A. M., Hlywiak, J., Hu, W., Peng, Z., Day, D. A., Knote, C., Brune, W. H., De Gouw, J. A., and Jimenez, J. L.: Modeling the Radical Chemistry in an Oxidation Flow Reactor: Radical Formation and Recycling, Sensitivities, and the OH Exposure Estimation Equation, The Journal of Physical Chemistry A, 119, 150406123535 006, 2015a.

Li, R., Palm, B. B., Ortega, A. M., Hlywiak, J., Hu, W., Peng, Z., Day, D. A., Knote, C., Brune, W. H., De Gouw, J. A., and Jimenez, J. L.: Modeling the Radical Chemistry in an Oxidation Flow Reactor: Radical Formation and Recycling, Sensitivities, and the OH Exposure Estimation Equation, The Journal of Physical Chemistry A, 119, 4418–4432, 2015b.

Mao, J., Ren, X., Brune, W., Olson, J., Crawford, J., Fried, A., Huey, L., Cohen, R., Heikes, B., and Singh, H.: Airborne measurement of OH reactivity during INTEX-B, Atmospheric Chemistry and Physics, 9, 163–173, 2009.

Peng, Z. and Jimenez, J. L.: Modeling of the chemistry in oxidation flow reactors with high initial NO, Atmospheric Chemistry and Physics, 17, 11 991–12 010, https://doi.org/10.5194/acp-17-11991-2017, 2017.

Peng, Z. and Jimenez, J. L.: KinSim: A Research-Grade, User-Friendly, Visual Kinetics Simulator for Chemical-Kinetics and Environmental-Chemistry Teaching, J. Chem. Educ., 96, 806–811, https://doi.org/10.1021/acs.jchemed.9b00033, 2019.

Peng, Z. and Jimenez, J. L.: Radical chemistry in oxidation flow reactors for atmospheric chemistry research, Chem. Soc. Rev., http://dx.doi.org/10.1039/C9CS00766K, 2020.

Peng, Z., Day, D. A., Stark, H., Li, R., Lee-Taylor, J., Palm, B. B., Brune, W. H., and Jimenez, J. L.: HO_x radical chemistry in oxidation flow reactors with low-pressure mercury lamps systematically examined by modeling, Atmospheric Measurement Techniques, 8, 4863–4890, 2015.

Peng, Z., Day, D. A., Ortega, A. M., Palm, B. B., Hu, W., Stark, H., Li, R., Tsigaridis, K., Brune, W. H., and Jimenez, J. L.: Non-OH chemistry in oxidation flow reactors for the study of atmospheric chemistry systematically examined by modeling, Atmospheric Chemistry and Physics, 16, 4283–4305, https://doi.org/10.5194/acp-16-4283-2016, http://www.atmos-chem-phys.net/16/4283/2016/, 2016.

Peng, Z., Palm, B. B., Day, D. A., Talukdar, R. K., Hu, W., Lambe, A. T., Brune, W. H., and Jimenez, J. L.: Model Evaluation of New Techniques for Maintaining High-NO Conditions in Oxidation Flow Reactors for the Study of OH-Initiated Atmospheric Chemistry, ACS Earth Space Chem., 2, 72–86, https://doi.org/10.1021/acsearthspacechem.7b00070, 2018.

Peng, Z., Lee-Taylor, J., Orlando, J. J., Tyndall, G. S., and Jimenez, J. L.: Organic peroxy radical chemistry in oxidation flow reactors and environmental chambers and their atmospheric relevance, Atmospheric Chemistry and Physics, 19, 813–834, https://doi.org/10.5194/acp-19-813-2019, 2019.

Serralheiro, C., Duflot, D., da Silva, F. F., Hoffmann, S. V., Jones, N. C., Mason, N. J., Mendes, B., and Limão-Vieira, P.: Toluene Valence and Rydberg Excitations as Studied by ab initio Calculations and Vacuum Ultraviolet (VUV) Synchrotron Radiation, J. Phys. Chem. A, 119, 9059–9069, https://doi.org/10.1021/acs.jpca.5b05080, https://doi.org/10.1021/acs.jpca.5b05080, 2015.

Spicer, D.: Germicidal Lamp Basics, https://www.light-sources.com/wp-content/uploads/2015/05/Germicidal_Lamp_Basics_-_2013.pdf, 2013.

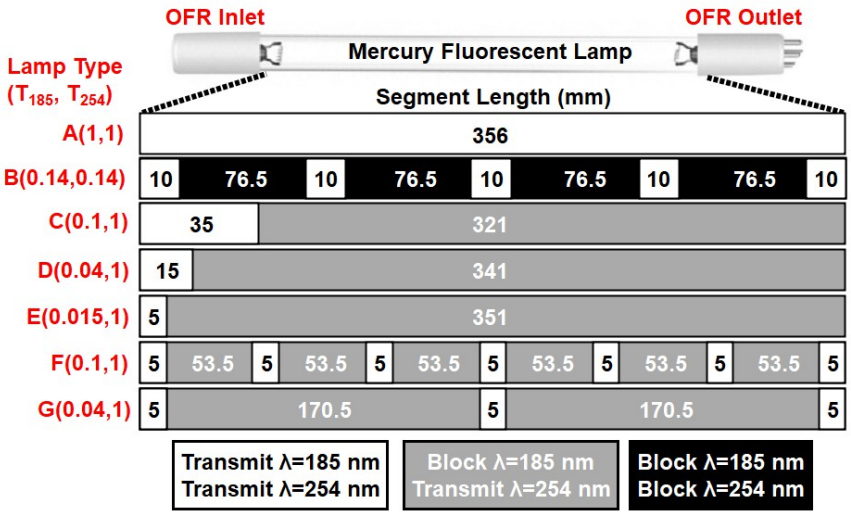

Figure 1. Low-pressure Hg fluorescent lamp types used in this study. Each lamp type contains 356 mm of quartz material that either transmits both λ = 185 and 254 nm radiation (white, T_{185} = 1), blocks λ = 185 nm and transmits λ = 254 nm radiation (grey, T_{185} = 0), or blocks both λ = 185 and 254 nm radiation (black, T_{185} = 0).

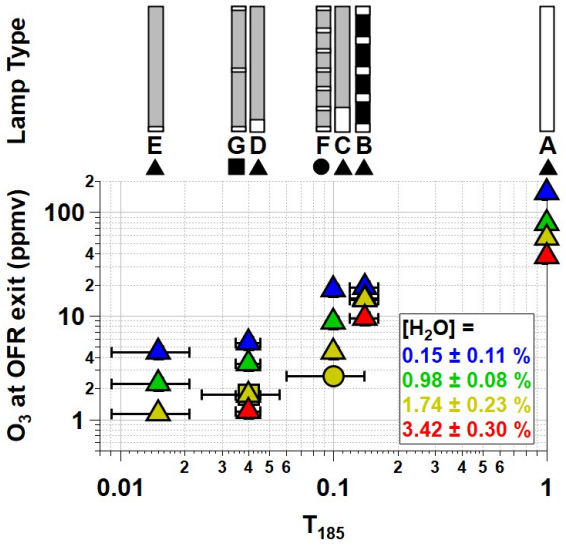

Figure 2. O_3 mixing ratio generated using OFR185 at I_{254} = (3.5±0.7)×10^{15} photons cm^{-2} s^{-1} (lamp types A and C-G) and I_{254} = 5.8×10^{14} photons cm^{-2} s^{-1} (lamp type B) as a function of T_{185} and [H_2O]. Error bars represent ±1σ of replicate O_3 measurements and ± 2 mm uncertainty in lengths of individual T_{185} = 0 and 1 segments.

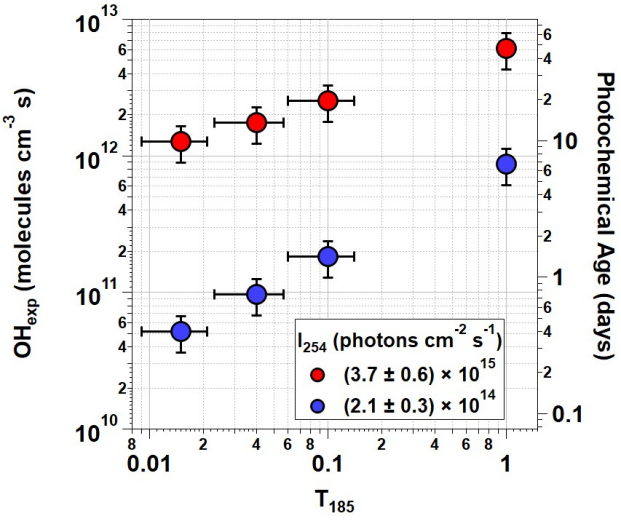

Figure 3. OH_{exp} generated using OFR185 ([H_2O] = 1.90±0.26%) at minimum and maximum I_{254} for each T_{185} value. Corresponding photochemical age shown on right y-axis assuming mean [OH] = 1.5×10^6 molec cm^{-3} (Mao et al., 2009). Error bars assume ± 30% uncertainty in OH_{exp} and ± 2 mm uncertainty in lengths of individual T_{185} = 0 and 1 segments.

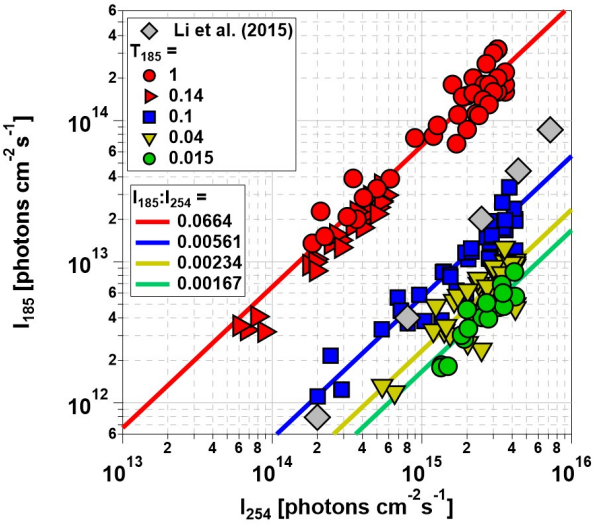

Figure 4. Calculated I_{185} and I_{254} values for the lamp types shown in Figure 1. I_{185}:I_{254} values were calculated from linear regression functions and used to derive OH_{ex} estimation equations. I_{185} and I_{254} values obtained by Li et al. (2015a) in an earlier-generation PAM OFR are shown for reference.

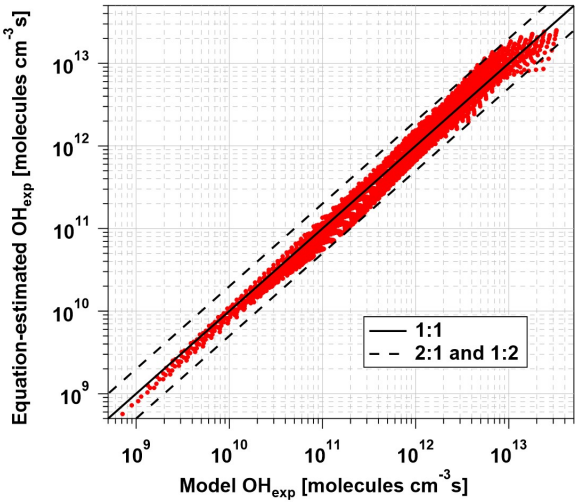

Figure 5. OH_{exp} calculated from the estimation equation (Eq. 1) as a function of OH_{exp} calculated from the full OFR185 KinSim mechanism (Table S1) for lamp types A and B. Solid and dashed lines correspond to the 1:1 and the 1:2 and 2:1 lines, respectively. Estimation equation fit coefficients are shown in Table 2.

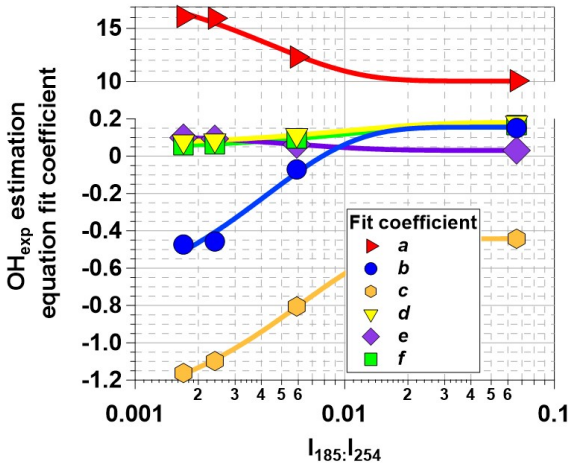

Figure 6. OH_{exp} estimation equation fit coefficients plotted as a function I_{254}:I_{254}. Trendlines were calculated from exponential regression functions with fit parameters that are presented in Table 3.

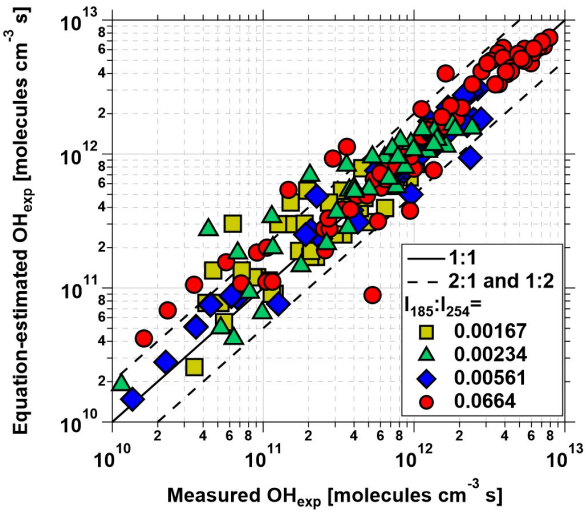

Figure 7. OH_{exp} calculated from estimation equation (Eq. 1 and Table 2) as a function of OH_{exp} calculated from tracer decay method for Hg lamp types with I_{254}:I_{254} values specified in legend.

Table 1. OFR conditions input to photochemical model.

P (mbar)	1013
T (°C)	22.5-31.9
Residence time (s)	63, 124, 251
H_2O (%)	0.03-3.9
O_3 (ppmv)	0.4-156
CO (ppmv)	0 or 6-9
SO_2 (ppbv)	0 or 288-629
I_{185} (photons cm^{-2} s^{-1})	1.1×10^{12}-3.2×10^{14}
I_{254} (photons cm^{-2} s^{-1})	6.0×10^{13}-4.2×10^{15}

Table 2. OH_{exp} estimation equation coefficients ($\pm1\sigma$) as defined in Eq. 1).

I_{185}:I_{254}	Coefficient					
	a	b	c	d	e	f
0.00167	16.109 ± 0.321	-0.4734 ± 0.0382	-1.1613 ± 0.0182	0.079284 ± 0.00105	0.99503 ± 0.00195	0.059251 ± 0.00115
0.00242	15.949 ± 0.347	-0.45692 ± 0.0398	-1.0974 ± 0.0186	0.084855 ± 0.0012	0.093976 ± 0.00206	0.064116 ± 0.00134
0.00595	12.306 ± 0.42	-0.070275 ± 0.04130	-0.8052 ± 0.0227	0.11347 ± 0.00249	0.062916± 0.00233	0.094896 ± 0.00291
0.0664	10.098 ± 0.576	0.15062 ± 0.0455	-0.44244 ± 0.0329	0.18041 ± 0.00872	0.031146 ± 0.00265	0.1672 ± 0.00953

Table 3. Parameterization of Eq. 1 coefficients ($\pm1\sigma$): y0 + A $\times$ exp[I_{185} : I_{254}) $\times$ invTau].

Coefficient	y0	A	invTau
a	10.053 ± 0.593	9.4455 ± 1.52	230.41 ± 71.8
b	0.15553 ± 0.0641	-0.99468 ± 0.168	237.54 ± 76.9
c	0.44174 ± 0.0106	-0.95747 ± 0.0223	163.04 ± 8.41
d	0.18069 ± 0.000904	-0.12054 ± 0.00161	98.577 ± 3.91
e	0.031037 ± 0.00208	0.094968 ± 0.00462	182.31 ± 18.8
f	0.16754 ± 0.00167	-0.1287 ± 0.00295	96.245 ± 6.65